Article:
Tonndorf, P., Del Pozo-Zamudio, O., Gruhler, N. et al. (8 more authors) (2017) On-chip waveguide coupling of a layered semiconductor single photon source. Nano Letters, 17 (9). pp. 5446-5451. ISSN 1530-6984

https://doi.org/10.1021/acs.nanolett.7b02092

On-chip waveguide coupling of a layered semiconductor single-photon source

Philipp Tonndorf[1,†], Osvaldo Del Pozo-Zamudio[1,†], Nico Gruhler[1,†], Johannes Kern[1], Robert Schmidt[1], Alexander I. Dmitriev[2], Anatoly P. Bakhtinov[2], Alexander I. Tartakovskii[3], Wolfram Pernice[1], Steffen Michaelis de Vasconcellos[1], and Rudolf Bratschitsch[1]*

[1] Institute of Physics and Center for Nanotechnology, University of Münster, 48149 Münster, Germany
[2] I. M. Frantsevich Institute for Problems of Material Science, NASU, Kiev-142, Ukraine
[3] Department of Physics and Astronomy, University of Sheffield, Sheffield S3 7RH, United Kingdom

[†]These authors contributed equally to this work

ABSTRACT:

Fully integrated quantum technology based on photons is in the focus of current research, because of its immense potential concerning performance and scalability. Ideally, the single-photon sources, the processing units, and the photon detectors are all combined on a single chip. Impressive progress has been made for on-chip quantum circuits and on-chip single-photon detection. In contrast, non-classical light is commonly coupled onto the photonic chip from the outside, because presently only few integrated single-photon sources exist. Here, we present waveguide-coupled single-photon emitters in the layered semiconductor gallium selenide as promising on-chip sources. GaSe crystals with a thickness below 100 nm are placed on Si_3N_4 rib or slot waveguides, resulting in a modified mode structure efficient for light coupling. Using optical excitation from within the Si_3N_4 waveguide, we find non-classicality of generated photons routed on the photonic chip. Thus, our work provides an easy-to-implement and robust light source for integrated quantum technology.

KEYWORDS: single-photon source, layered material, GaSe, on-chip waveguiding

The availability of efficient and robust single-photon emitters in large numbers constitutes one of the most stringent roadblocks for current photonic technology. For chip-based systems, the sources should be waveguide coupled to interface directly with integrated optical or nanophotonic devices. Such devices have been shown to provide potential for scalability, which is essential for viable applications in quantum technologies. When working with a monolithic material platform, self-assembled semiconductor quantum dots embedded into GaAs waveguides[1–3] or color centers integrated in diamond nanophotonic structures[4,5] have been used as on-chip single-photon sources. Alternatively, near field coupling of nanoscale single-photon emitters to prefabricated waveguides allowed for hybrid quantum photonic devices. In this way, single photons have been extracted from color centers in diamond[6,7], semiconductor quantum dots[8], single-walled carbon nanotubes[9] or defect centers in hexagonal boron nitride[10,11] placed on or in dielectric waveguides (see supplementary section 1 for an overview). The latter belong to the newly discovered class of robust solid-state single-photon sources in layered crystals. Bright and stable single-photon emitters have further been demonstrated in 2D transition metal dichalcogenides[12–17] and the semiconductor GaSe[18], where single-photon emission arises from strain-induced potential wells in the layered crystal. In this work, we couple GaSe crystals with incorporated quantum emitters to dielectric waveguides to create on-chip single-photon sources, from which non-classical light can be extracted via focusing grating couplers.

Figures 1a and b present an artistic impression of the fabricated sample. The GaSe crystal (red) is transferred with a stamping technique[19] onto the Si_3N_4 rib waveguide (WG) with grating couplers at both ends (see methods for fabrication details). The 90 nm thick GaSe crystals bend around the Si_3N_4 rib waveguide, as evident from the optical and atomic force micrograph (Fig. 1c-e and supplementary information section 2). A confocal micro-photoluminescence (PL) image of the sample (Fig. 1f and methods) shows strong light emission from the GaSe crystal, but also at the

position of the grating couplers. The PL spectrum measured at low temperatures (T = 10 K) at the coupler is similar to the spectrum of the GaSe crystal lying on the flat substrate (Fig. 1g). Therefore, we attribute the light detected at the grating coupler to PL from the GaSe crystal, which has been excited by laser light coupled into the rib waveguide via the same coupler. This measurement thus shows that PL from the GaSe crystal couples into the waveguide and is routed with low scattering and absorption losses (4,4 dB/cm) to the grating coupler.

To study the nature of the wave guiding, we spatially separate the excitation and detection sites on the sample (see methods). The laser excitation is fixed at one position, while we scan the point of detection across a large area of the sample. First, we place the excitation spot on the left coupler, as shown in the PL map of another GaSe crystal on a Si_3N_4 slot waveguide (Fig. 2a and Fig. S1). Grey circles indicate the locations, where individual PL spectra are recorded (Fig. 2b). The spectrum detected at the left coupler (i) exhibits several narrow emission lines. Interestingly, we detect the same spectral features also from the right coupler (v), although the major part of the linear Si_3N_4 waveguide is covered by the GaSe crystal. This illustrates that wave guiding is not prohibited, if GaSe with a high refractive index is placed on top of the waveguide.

To understand the excitation mechanism of the light emitters incorporated in the GaSe crystal, we simulate the optical mode profiles of the photonic nanostructure using finite element methods (FEM) (see methods). The fundamental modes of the rib and slot waveguides show highest intensity in the center of the waveguide and in the slot, respectively (Fig. 2c and d). This renders the excitation of the waveguide surroundings very inefficient. The situation changes drastically, if a GaSe crystal with a thickness of several tens of nanometers is placed on top of the linear dielectric waveguide. Because of the large refractive index of GaSe (n = 2.8 - 3.1) [20] compared to Si_3N_4 (n = 2) [21], the fundamental mode is pulled into the GaSe material (Fig. 2e and f). This way, the localized emission centers can be efficiently excited in vicinity of the Si_3N_4 waveguide. The

emitted PL signal couples back into the same linear waveguide and is transmitted to the grating couplers at both ends.

Obviously, not all of the emitted light couples into the waveguide and part of it leaves the thin GaSe flake (Fig. 2a). Therefore, the same spectral features measured at the grating couplers can also be found at the edge of the GaSe crystal. For example, the prominent emission feature at 2.025 eV originates from position (ii) on the GaSe flake, while the emission line at 1.983 eV stems from position (iii). Both emission characteristics can also be found at folds and the edges of the GaSe crystal (e.g. at position (iv)). Indeed, the thin GaSe crystal itself acts as a slab waveguide for the emitted PL. To verify that the GaSe crystal itself works as a waveguide, we move the excitation spot to emitter #2 (green arrow in Fig. 3a). Consequently, the two grating couplers (i) and (iv) light up with the same PL spectrum as the excited emitter #2 at position (ii) (Fig. 3b). Again, the PL signal from emitter #2 can also be detected at folds in the GaSe crystal and at the edge (iii). If the excitation spot is moved to yet another emitter, the PL of this emitter (but not the others) can be detected at both couplers and the edge of the GaSe flake (see supplementary Fig. S2). This behavior indicates that the GaSe crystal does not efficiently guide the laser light used for excitation at 2.33 eV, but only the PL light at lower photon energies. This effect is due to the low absorption coefficient of 0.25 cm^{-1} (1 dB/cm absorption loss) below the absorption edge of GaSe at 2.08 eV [22]. Hence, the emitted PL light can travel almost unattenuated through the thin GaSe crystal. The wave guiding ability of the GaSe crystal itself is intimately linked to its thickness. Wave guiding ceases for GaSe thicknesses less than about 50 nm (see supplementary Fig. S3). Therefore, we deposit GaSe flakes with thicknesses around 90 nm for optimum coupling efficiency.

The amount of light, which is confined inside the GaSe crystal, also strongly depends on the orientation of the emission dipole and the location of the emitter inside the thin GaSe flake. The

FEM simulations show that the PL trapped in the GaSe crystal preferably couples to the linear Si_3N_4 waveguide, so that up to 45 % of the entire emitted PL can be confined in the hybrid GaSe/Si_3N_4 waveguide structure (Fig. 3c and supplementary Fig. S4 and S5). This one-dimensional confinement is the reason why a strong PL signal is still observed at both grating couplers, although the GaSe flake covers the major part of the Si_3N_4 waveguide. At the edge of the GaSe flake roughly half of the light couples into the bare Si_3N_4 waveguide. Therefore, in total, up to 21 % of the emission can be collected in the on-chip waveguide (Fig. 3c). For a rib waveguide without slot, the highest simulated coupling efficiency amounts to 15% (see supplementary Fig. S5). From the experiment, we can estimate a lower limit of the coupling efficiency of the emitter shown in Fig. 3b into the bare waveguide to 3.5 % (see supplementary section 8).

In our experiment, the PL signal is directed into free-space by the grating coupler at the end of the rib waveguide (Fig. 3d). By examining many emission centers (30) in the GaSe crystal positioned on top of the Si_3N_4 waveguide, we find that the measured PL intensity at the coupler is up to twice as high compared to detection directly at the emitter position in free-space (I_{direct}). In our confocal scanning microscope, we collect only a small fraction (spot size of 1 µm²) of the light scattered out at the grating couplers, which have a large footprint of 200 μm^2. To determine the total intensity output of the grating couplers, we therefore integrate the PL intensity ($I_{coupler}$) of the entire coupler area of the PL map in Fig. 3a. $I_{coupler}$ is about 80 times higher than I_{direct} of a 1 µm² area at the emitter position (ii). With a typical out-coupling efficiency of the grating coupler of 50 % [23] (Fig. 3d), we can estimate that at least 160 times more PL is coupled into the waveguide compared to the confocal measurement of this emitter directly from the top. Consequently, the photon count rate from the single emitter could be significantly enhanced by 2

orders of magnitude by using on-chip light detectors instead of free-space detection with a confocal laser scanning setup and the grating couplers.

The coupled light emitter of Fig. 3b exhibits the typical signature for a localized exciton and its biexciton on the low-energy side [18]. To prove that the localized exciton is a single-photon emitter, we measure the photon statistics with a Hanbury Brown and Twiss setup. The second-order correlation function $g^{(2)}(\tau)$ of the emission line at 1.983 eV is depicted in Fig. 4 for four different configurations, including both excitation and detection from free-space and through the Si_3N_4 waveguide (see insets). In all configurations $g^{(2)}(\tau=0)$ is clearly below 0.5, which proves that the single-photon behavior is also preserved when routed via the on-chip rib waveguide. Remarkably, excitation and detection on the same grating coupler also works, which constitutes a new easy-to-use free-space single-photon source. As a result, the full suite of nanophotonic components can be employed to further process the emitted light.

For usability in quantum information technology it is important that the single-photon emitters can also be triggered by pulsed excitation. Therefore, we measure the second-order correlation function under pulsed excitation (supplementary Fig. S6), which also shows single-photon behavior with $g^{(2)}(0) = 0.24$.

Besides optical excitation, it should also be possible to pump[17,24] and control[16,17,24–26] the single-photon emitters electrically, since GaSe exhibits electroluminescence[27]. For deterministic positioning of the single-photon emitters on the nanoscale, one could create an artificial strain profile to induce their creation[28–30]. Finally, the generation of indistinguishable photons is important. They must have the same polarization, energy, and the emission needs to be coherent. The polarization of the emitters could be controlled by strain[28] or dictated by the waveguide itself. The energy and coherence are directly linked to the line width of the emitters, which could

be further decreased by using free-standing layers[12], depositing them on single-crystalline substrates[31], or sandwiching them by a wide band-gap material[32].

In conclusion, we have presented on-chip coupling of single-photon emitters incorporated in thin GaSe crystals to nanophotonic waveguides. The optical properties of the GaSe crystal result in a modified hybrid mode structure efficient for light coupling. The hybrid integration of passive photonic circuitry with active single-photon emitters decouples the implementation of the desired light sources from the realization of the scalable quantum photonic architecture. In that way, material and processing incompatibilities during fabrication can be efficiently avoided. Furthermore, layered 2D materials will allow for upscaling with parallel transfer techniques or direct growth on the photonic chip. Thus, this new class of on-chip single-photon sources based on layered materials facilitates integrated quantum technology.

METHODS:

Sample Fabrication

The substrate for the photonic chip consists of a 200nm Si_3N_4 layer grown by low-temperature chemical vapor deposition on top of a SiO_2 (2 µm)/Si wafer. The photonic nanostructures in the Si_3N_4 layer are fabricated by electron-beam lithography and a CHF_3/O_2-based dry etching step. In between, a reflow procedure is applied to the e-beam resist to realize low-loss waveguiding structures[33]. 500 nm wide and 150 nm high rib waveguides are created, leaving 50 nm of Si_3N_4 on the substrate (Fig. 1b). To increase the coupling efficiency, we also fabricate slot waveguides with a 75 nm wide slot between two 250 nm wide waveguides (see supplementary Fig. S1). At both ends of the linear waveguide, grating couplers scatter light out of the sample plane via second-order Bragg diffraction. The grating couplers are designed for light in the visible regime and have the shape of an isosceles triangle extending over 24 µm x 17 µm leading to a footprint of around 200 µm². To increase the out-coupling efficiency, a second e-beam lithography step is used to deposit a 775 nm thick hydrogen silsesquioxane (HSQ) layer selectively on top of both couplers[23].

Gallium selenide single crystals are grown by high-pressure vertical zone melting in graphite crucibles in Ar atmosphere. 90 - 100 nm thick GaSe flakes with lateral sizes of 10 – 100 µm are obtained by mechanical exfoliation of the single crystal and are transferred with a polymer stamp onto the linear Si_3N_4 waveguides[19] (Fig. 1d).

Photoluminescence and Photon Correlation Measurements

The samples are placed in a Helium-flow cryostat (T = 10 K) and examined in reflection geometry with a laser scanning confocal microscope[12]. For excitation, light from a continuous wave laser with a wavelength of 532 nm and power densities between 200 and 8000 W/cm² is focused on the sample with an objective lens (numerical aperture NA = 0.75). To separate the

excitation and detection area on the sample, a second excitation path is added by inserting a beam splitter in front of the objective lens. In that way, a fixed excitation spot can be freely positioned on the sample, while the photoluminescence (PL) signal of the sample can be scanned in an area of 200 µm x 200 µm. The collected PL light is filtered with a 560 nm longpass and is either sent to an avalanche photodiode (APD) or a monochromator with a focal length of 750 mm. At one exit slit of the monochromator a thermoelectrically cooled, back-illuminated deep-depletion charge-coupled device (CCD) is attached. At the other exit slit, a Hanbury Brown and Twiss setup is attached, consisting of a 50:50 beam splitter and two APDs with a time resolution of 50 ps. The integration times and obtained number of coincidences for $g^{(2)}(\tau)$ shown in Fig.4 range between 7 h with 40 coincidences and 31 h with 100 coincidences. The count rates on each APD of the HBT setup amounts to 4 kcps. With a measured transmission efficiency of 4.5 % of our laser scanning confocal microscope and an APD detection efficiency of 40 % we can estimate the collected intensity of the single-photon emitters by the objective lens to be 220 kcps.

Electromagnetic Simulation

The finite element method (FEM) simulations are performed with the software Comsol (https://www.comsol.com) using the RF module and frequency domain emw package. The simulations are carried out using built-in wavelength-dependent refractive indices for the materials in our system. The optical modes are evaluated by mode analysis at an energy of 2.33 eV ($\lambda_{excitation}$ = 532 nm). To study the propagation of the PL, an electric point dipole with λ = 625 nm is placed in the GaSe crystal. In Fig. 3 the modulus of the Poynting vector |S| is plotted, which represents the time-averaged power flow.

ASSOCIATED CONTENT

Supporting Information

More detailed information about the waveguide geometry and the light propagation in the hybrid system for different crystal thicknesses and emitter polarizations.

AUTHOR INFORMATION

Corresponding Author

E-mail: Rudolf.Bratschitsch@uni-muenster.de

ORCID

Rudolf Bratschitsch: 0000-0002-2368-2548

Steffen Michaelis de Vasconcellos: 0000-0003-3584-0635

Robert Schmidt: 0000-0002-8856-3347

Notes

The authors declare no competing financial interest.

ACKNOWLEDGMENTS

A.I.T. was supported by the EPSRC grant EP/M012727/1, Graphene Flagship under grant agreement 696656, ITN Spin-NANO under grant agreement 676108, and ITN 4PHOTON under grant agreement 721394.

REFERENCES

(1) Englund, D.; Faraon, A.; Zhang, B.; Yamamoto, Y.; Vucković, J. Opt. Express **2007**, 15, 5550–5558.

(2) Dietrich, C. P.; Fiore, A.; Thompson, M. G.; Kamp, M.; Höfling, S. Laser Photonics Rev. **2016**, 10, 870–894.

(3) Reithmaier, G.; Kaniber, M.; Flassig, F.; Lichtmannecker, S.; Müller, K.; Andrejew, A.; Vuckovic, J.; Gross, R.; Finley, J. J. Nano Lett. **2015**, 15, 5208–5213.

(4) Greentree, A. D.; Fairchild, B. A.; Hossain, F. M.; Prawer, S. Mater. Today **2008**, 11, 22–31.

(5) Hausmann, B. J. M.; Shields, B.; Quan, Q.; Maletinsky, P.; McCutcheon, M.; Choy, J. T.; Babinec, T. M.; Kubanek, A.; Yacoby, A.; Lukin, M. D.; et al. Nano Lett. **2012**, 12, 1578–1582.

(6) Fu, K. M. C.; Santori, C.; Barclay, P. E.; Aharonovich, I.; Prawer, S.; Meyer, N.; Holm, A. M.; Beausoleil, R. G. Appl. Phys. Lett. **2008**, 93, 234107.

(7) Schell, A. W.; Kaschke, J.; Fischer, J.; Henze, R.; Wolters, J.; Wegener, M.; Benson, O. Sci. Rep. **2013**, 3, 1577.

(8) Zadeh, I. E.; Elshaari, A. W.; Jöns, K. D.; Fognini, A.; Dalacu, D.; Poole, P. J.; Reimer, M. E.; Zwiller, V. Nano Lett. **2016**, 16, 2289–2294.

(9) Khasminskaya, S.; Pyatkov, F.; Słowik, K.; Ferrari, S.; Kahl, O.; Kovalyuk, V.; Rath, P.; Vetter, A.; Hennrich, F.; Kappes, M. M.; et al. Nature **2016**, 10, 727–732.

(10) Tran, T. T.; Bray, K.; Ford, M. J.; Toth, M.; Aharonovich, I. Nat. Nanotechnol. **2016**, 11, 37–42.

(11) Schell, A. W.; Takashima, H.; Tran, T. T.; Aharonovich, I.; Takeuchi, S. ACS Photonics **2017**, 4, 761–767.

(12) Tonndorf, P.; Schmidt, R.; Schneider, R.; Kern, J.; Buscema, M.; Steele, G. A.; Castellanos-Gomez, A.; van der Zant, H. S. J.; Michaelis de Vasconcellos, S.; Bratschitsch, R. Optica **2015**, 2, 347–352.

(13) Srivastava, A.; Sidler, M.; Allain, A. V.; Lembke, D. S.; Kis, A.; Imamoğlu, A. Nat. Nanotechnol. **2015**, 10, 491–496.

(14) Koperski, M.; Nogajewski, K.; Arora, A.; Cherkez, V.; Mallet, P.; Veuillen, J.-Y.; Marcus, J.; Kossacki, P.; Potemski, M. Nat. Nanotechnol. **2015**, 10, 503–506.

(15) He, Y.; Clark, G.; Schaibley, J. R.; He, Y.; Chen, M.-C.; Wei, Y.-J.; Ding, X.; Zhang, Q.; Yao, W.; Xu, X.; et al. Nat. Nanotechnol. **2015**, 10, 497–502.

(16) Chakraborty, C.; Kinnischtzke, L.; Goodfellow, K. M.; Beams, R.; Vamivakas, a. N. Nat. Nanotechnol. **2015**, 10, 507–511.

(17) Berraquero, C. P.; Barbone, M.; Kara, D. M.; Chen, X.; Goykhman, I.; Yoon, D.; Ott, A. K.; Beitner, J.; Watanabe, K.; Taniguchi, T.; et al. Nat. Commun. **2016**, 7, 12978.

(18) Tonndorf, P.; Schwarz, S.; Kern, J.; Niehues, I.; Zamudio, O. D. P.; Dmitriev, A.; Bakhtinov, A.; Borisenko, D.; Kolesnikov, N.; Tartakovskii, A.; et al. 2D Mater. **2017**, 4, 21010.

(19) Castellanos-Gomez, A.; Buscema, M.; Molenaar, R.; Singh, V.; Janssen, L.; van der Zant, H. S. J.; Steele, G. a. 2D Mater. **2014**, 1, 11002.

(20) Edward D. Palik. Handbook of Optical Constants of Solids; 1997.

(21) Philipp, H. R. J. Electrochem. Soc. **1973**, 120, 295–300.

(22) Singh, N. B.; Suhre, D. R.; Balakrishna, V.; Marable, M.; Meyer, R.; Road, B. Prog. Cryst. Growth Charact. Mater. **1998**, 37, 47–102.

(23) Taillaert, D.; Van Laere, F.; Ayre, M.; Bogaerts, W.; Van Thourhout, D.; Bienstman, P.; Baets, R. Jpn. J. Appl. Phys. **2006**, 45, 6071–6077.

(24) Schwarz, S.; Kozikov, A.; Withers, F.; Maguire, J. K.; Foster, A. P.; Dufferwiel, S.; Hague, L.; Makhonin, M. N.; Wilson, L. R.; Geim, A. K.; et al. 2D Mater. **2016**, 3, 25038.

(25) Branny, A.; Wang, G.; Kumar, S.; Robert, C.; Lassagne, B.; Marie, X.; Gerardot, B. D.; Urbaszek, B. Appl. Phys. Lett. **2016**, 108, 142101.

(26) Chakraborty, C.; Goodfellow, K. M.; Dhara, S.; Yoshimura, A.; Meunier, V.; Vamivakas, N. Nano Lett. **2017**, 17, 2253–2258.

(27) Cingolani, A.; Levialdi, A. Cim. B **1968**, 55, 146–154.

(28) Kern, J. J.; Niehues, I.; Tonndorf, P.; Schmidt, R.; Wigger, D.; Schneider, R.; Stiehm, T.; Michaelis de Vasconcellos, S.; Reiter, D. E.; Kuhn, T.; et al. Adv. Mater. **2016**, 28, 7101–7105.

(29) Branny, A.; Kumar, S.; Proux, R.; Gerardot, B. D. Nat. Commun. **2017**, 8, 15053.

(30) Palacios-Berraquero, C.; Kara, D. M.; Montblanch, A. R.; Latawiec, P.; Yoon, D.; Ott, A. K.; Loncar, M.; Ferrari, A. C.; Atatüre, M. Nat. Commun. **2017**, 8, 15093.

(31) Iff, O.; He, Y.-M.; Lundt, N.; Stoll, S.; Baumann, V.; Höfling, S.; Schneider, C. Optica **2017**, 4, 669–673.

(32) Cadiz, F.; Courtade, E.; Robert, C.; Wang, G.; Shen, Y.; Cai, H.; Taniguchi, T.; Watanabe, K.; Carrere, H.; Lagarde, D.; et al. Phys. Rev. X **2017**, 7, 21026.

(33) Gruhler, N.; Benz, C.; Jang, H.; Ahn, J.-H.; Danneau, R.; Pernice, W. H. P. Opt. Express **2013**, 21, 31678–31689.

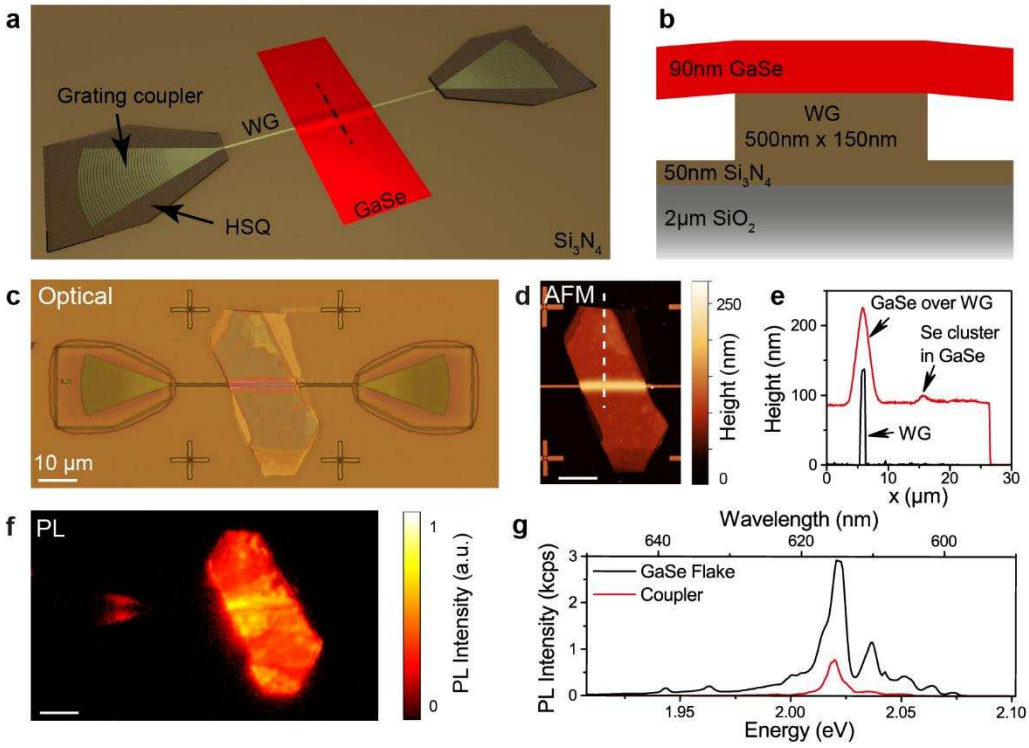

Figure 1. (a) Schematic illustration of a thin GaSe crystal on top of a linear dielectric photonic waveguide with two grating couplers. The HSQ layer on the couplers increases the out-of-plane coupling efficiency. (b) Schematic cross section at the position indicated by the black dashed line in (a). The GaSe flake is bent at the Si_3N_4 waveguide, which can be seen both in (c) the optical reflection and (d) atomic force micrograph (AFM). (e) The AFM height profile at the position indicated by the white dashed line in (e) yields a GaSe thickness of 90 nm (red line). Small islands with a height of 10 nm indicate the presence of Se clusters in the GaSe crystal. (f) The photoluminescence (PL) map reveals bright emission from the thin GaSe flake. GaSe PL can also be detected at the coupler positions, as demonstrated by the spectrum (g).

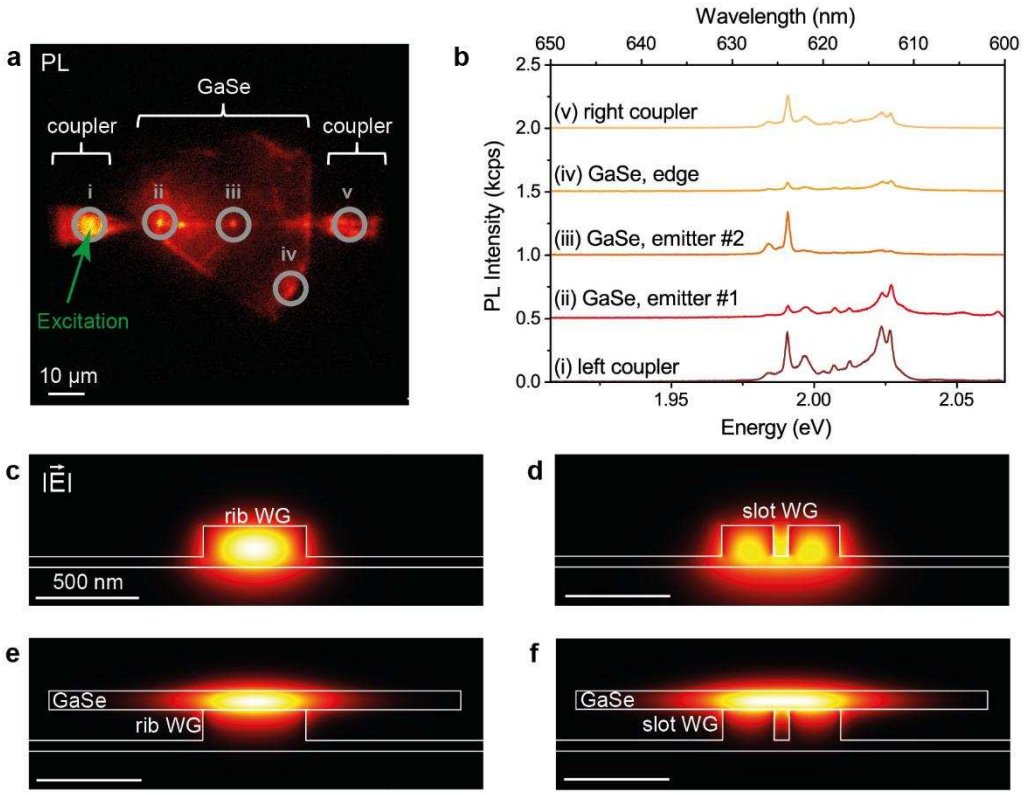

Figure 2. (a) In the photoluminescence (PL) map the excitation spot is placed onto the left grating coupler (green arrow). The detection spot is scanned over the sample. PL at the grating couplers and the edge of the GaSe flake is visible. (b) PL spectra measured at the locations indicated with the labels (i)-(v) in (a). (c, d) The simulations depict the mode profiles of a rib and a slot waveguide, respectively. (e, f) If the thin GaSe crystal is placed on the Si_3N_4 waveguide, the mode with the highest intensity is pulled into the GaSe material.

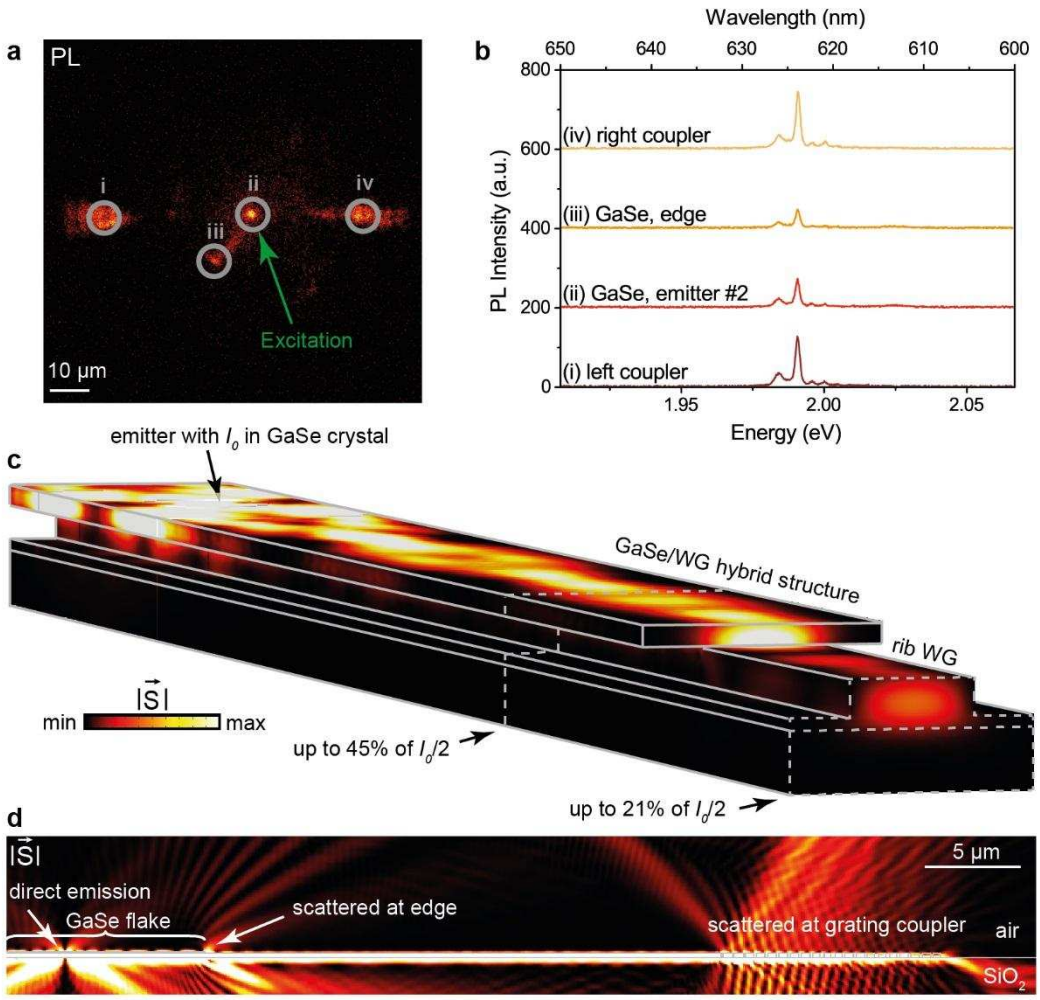

Figure 3. Photoluminescence (PL) light guiding with the GaSe/Si_3N_4 hybrid waveguide structure. (a) The excitation spot is placed at a localized emission center in the GaSe crystal (green arrow in the PL map). (b) At the GaSe flake and both couplers the same PL spectrum is measured, indicating that the GaSe crystal itself acts as a waveguide. (c) The 3D simulation shows the propagation of PL light (absolute value of the Poynting vector $|\vec{S}|$). A 1D confinement of up to 45% of the emitter intensity I_0 can be reached in the GaSe/Si_3N_4 hybrid structure. At the edge of the GaSe flake, half of the light couples into the bare Si_3N_4 rib waveguide (in total 21 % of I_0). (d) The 2D simulation with view from the side shows, where the PL is scattered out into the air, i.e. at the position of the emitter, at the edge of the thin GaSe crystal on the Si_3N_4 waveguide, and at the grating coupler.

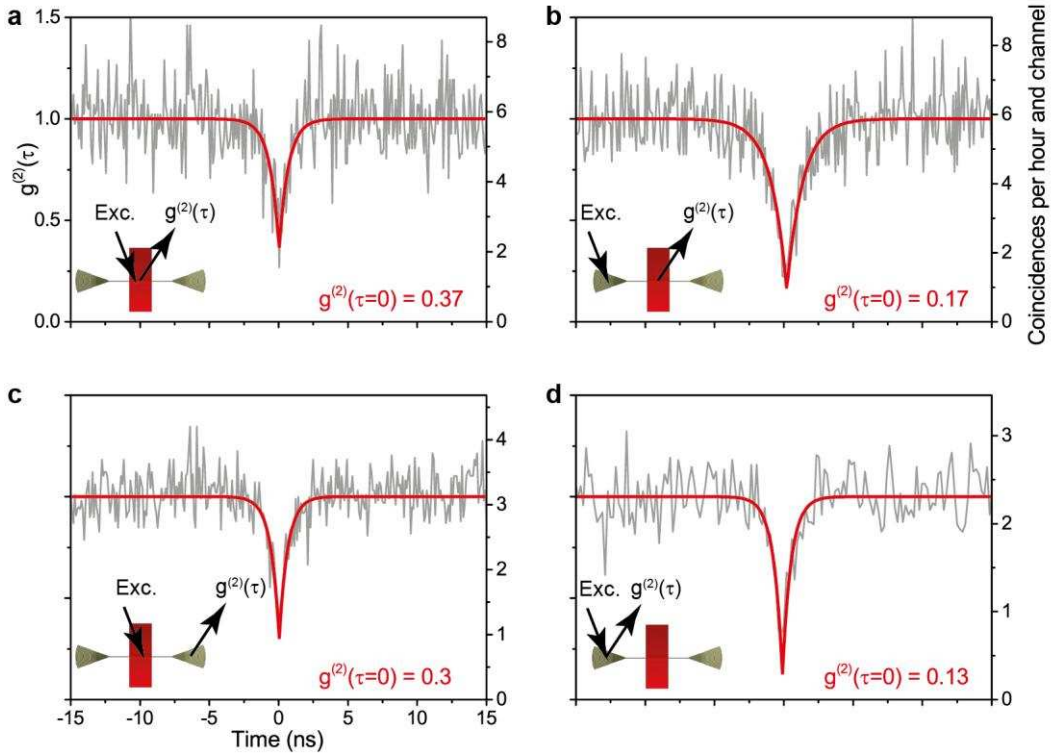

Figure 4. Free-space and waveguide-coupled single-photon emission of the localized emission center from Fig. 3 for different experimental configurations. (a) Excitation and detection spot are placed at the localized emitter in the GaSe crystal. (b) Excitation via the linear Si_3N_4 waveguide, and detection at the position of the localized emitter. (c) Excitation at the emitter and detection at the coupler. (d) Excitation and detection at the coupler. In every configuration the second-order correlation function $g^{(2)}(\tau = 0) < 0.5$, which proves the single-photon nature of the source.

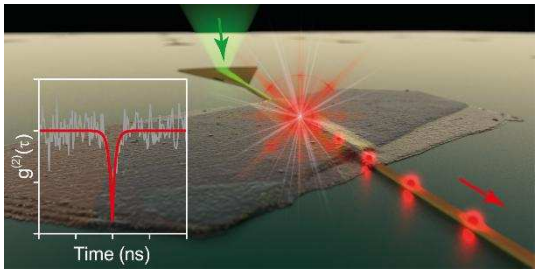

ToC Figure

Supporting Information

On-chip waveguide coupling of a layered semiconductor single-photon source

Philipp Tonndorf[1,†], Osvaldo Del Pozo-Zamudio[1,†], Nico Gruhler[1,†], Johannes Kern[1], Robert Schmidt[1], Alexander I. Dmitriev[2], Anatoly P. Bakhtinov[2], Alexander I. Tartakovskii[3], Wolfram Pernice[1], Steffen Michaelis de Vasconcellos[1], and Rudolf Bratschitsch[1]*

[1] Institute of Physics and Center for Nanotechnology, University of Münster, 48149 Münster, Germany
[2] I. M. Frantsevich Institute for Problems of Material Science, NASU, Kiev-142, Ukraine
[3] Department of Physics and Astronomy, University of Sheffield, Sheffield S3 7RH, United Kingdom

[†]These authors contributed equally to this work
*Rudolf.Bratschitsch@uni-muenster.de

Table of contents

1. Overview of coupled solid-state single-photon sources

Table S1. Comparison of coupled solid-state single-photon sources from refs 1, 3, 5, 7-9, and 11 of the manuscript and our work.

Ref.	Type of single-photon emitter	Hybrid structure	$g^{(2)}(0)$	Temperature	Excitation	Photon energy (eV)	Line width (meV)	Photolumi-nescence life time (ns)	Counts on detector	Coupling efficiency (Theoretical)	Coupling efficiency (Experimental)
1	exciton	QD in photonic crystal cavity	0.50	cryogenic	optical	1.330	86	0.116	-	0.98	-
3	exciton	QD in optical waveguide	0.36	cryogenic	optical	1.348	10	0.8	-	-	-
5	impurity/defect	NV center in ring resonator made of diamond	0.20	RT	optical	1.770	~250	~25	15.000 (in saturation)	-	-
7	impurity/defect	NV center in nanodiamond in photoresist written to microdiscs	0.37	RT	optical	1.770	~250	~25	23.000	-	-
8	exciton	QD in nanowire in waveguide	0.07	-	optical	1.412	0.014	1	-	0.24	0.36
9	exciton	CNT on optical waveguide	0.49	cryogenic	electrical	0.905	20 (RT)	0.07	8.000	-	-
11	impurity/defect	hBN on tapered fiber	0.15	RT	optical	1.862	6	20	36.000 (in saturation)	0.14	0.10
this work	exciton	GaSe crystal on optical waveguide	0.13	cryogenic	optical	1.984	2	1	4.000-10.000 (confocal)	0.21	0.035

2. Atomic force microscopy (AFM)

The AFM height profile measured along the white dotted line in Fig. 1e of the manuscript yields a GaSe thickness of 90 nm. The particular shape of the AFM line scan and the purple color of the GaSe crystal in proximity to the waveguide in the optical image of Fig. 1c indicate that the layered crystal is suspended close to the rectangular Si_3N_4 rib waveguide (Fig. 1b of the manuscript). The GaSe flake also exhibits several islands with a height around 10 nm, caused by selenium clusters in the GaSe crystal.

3. Schematic illustration of the Si_3N_4 slot waveguide with deposited GaSe crystal

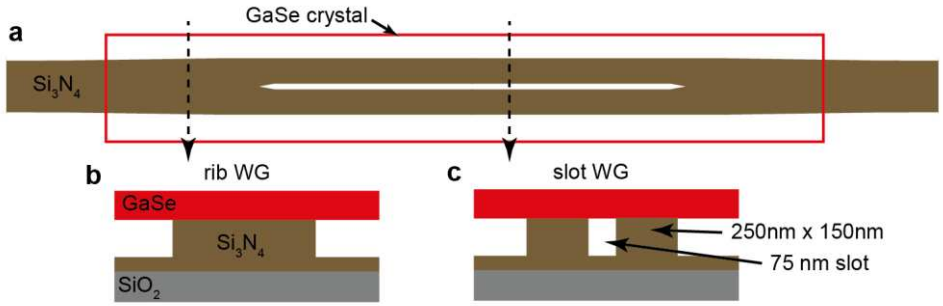

Figure S1. Schematic illustration of a slot waveguide (WG) with thin GaSe crystal on top. (a) Top view. The GaSe crystal (red line) covers the entire slot region. (b,c). Cross section of the structure at positions indicated with the black dotted lines in (A).

4. Wave guiding of the laser light used for excitation and the emitted photoluminescence (PL) in the thin GaSe crystal

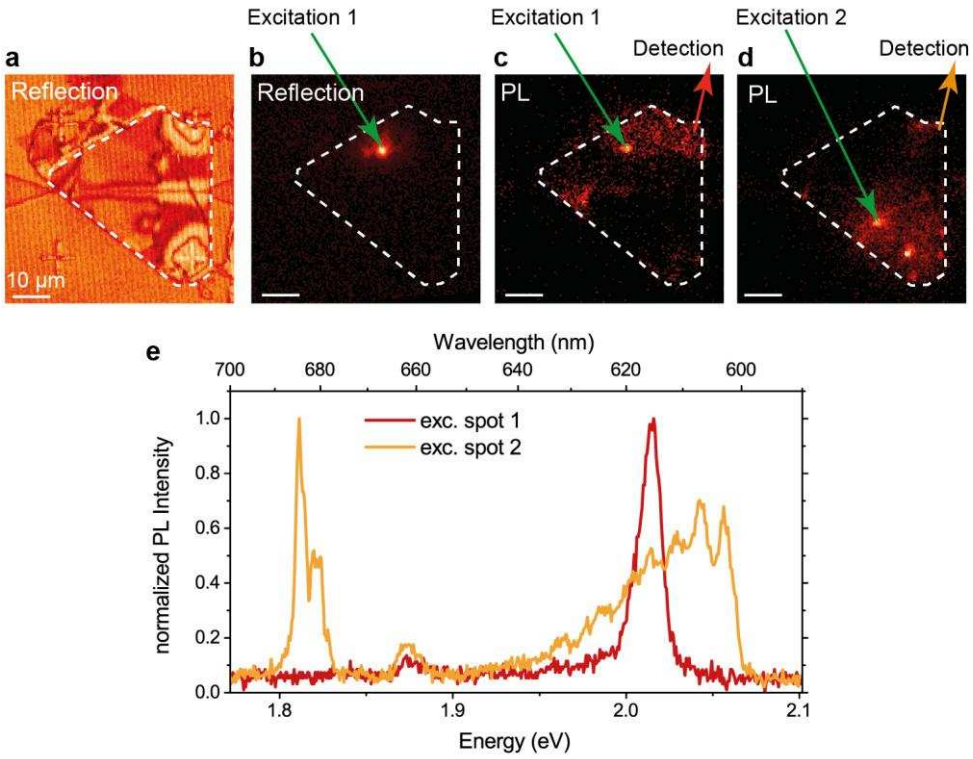

Figure S2. Wave guiding of the emitted PL in the GaSe flake. (a) Optical reflection image of the GaSe crystal on the Si_3N_4 slot waveguide, presented in Fig. 2 and 3 of the manuscript. (b) The laser spot is fixed at one position on the GaSe flake. Only the laser focus is visible, while the rest of the GaSe crystal remains dark, i.e the laser light used for excitation is not guided in the GaSe flake. (c,d) In contrast, other areas of the GaSe crystal light up in the photoluminescence (PL) map. (e) The spectra measured at the upper right corner of the GaSe crystal in Fig. S2c and d change, depending on the position of the excitation spot on the GaSe crystal. This is due to the wave guiding ability of the 90 nm thick GaSe crystal for PL light.

5. Propagation of the photoluminescence (PL) light in thin GaSe crystals of different thickness placed on bare Si_3N_4/SiO_2 substrate (without a linear Si_3N_4 waveguide)

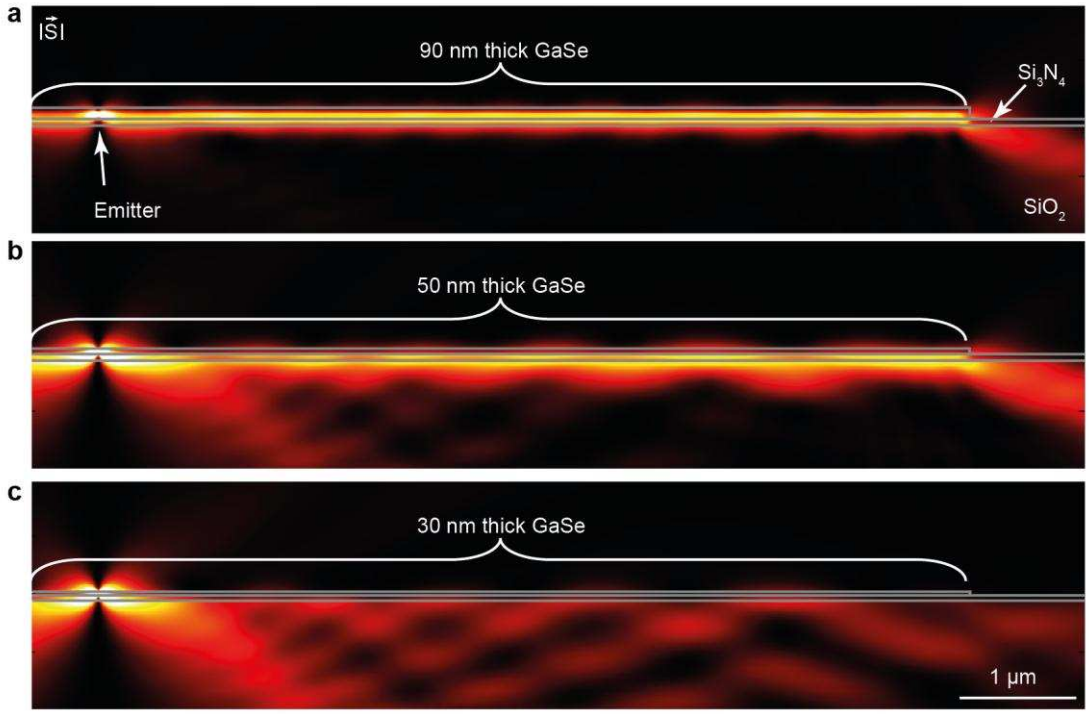

Figure S3. 2D simulation of the propagation of the emitted PL in the GaSe crystal depending on its thickness. The GaSe crystal is placed on the bare Si_3N_4/SiO_2 substrate without linear Si_3N_4 waveguide. (a) In a 90 nm thick GaSe crystal, the majority of the PL emission is confined and guided. (b) If the GaSe thickness is reduced to 50 nm, the confinement decreases and more light is scattered into the substrate. (c) If the thickness of the GaSe crystal is reduced to 30 nm, no coupling of the emitted PL into the GaSe flake is visible and the majority of the PL propagates into the substrate.

6. Propagation of the emitted photoluminescence in the hybrid waveguide structure

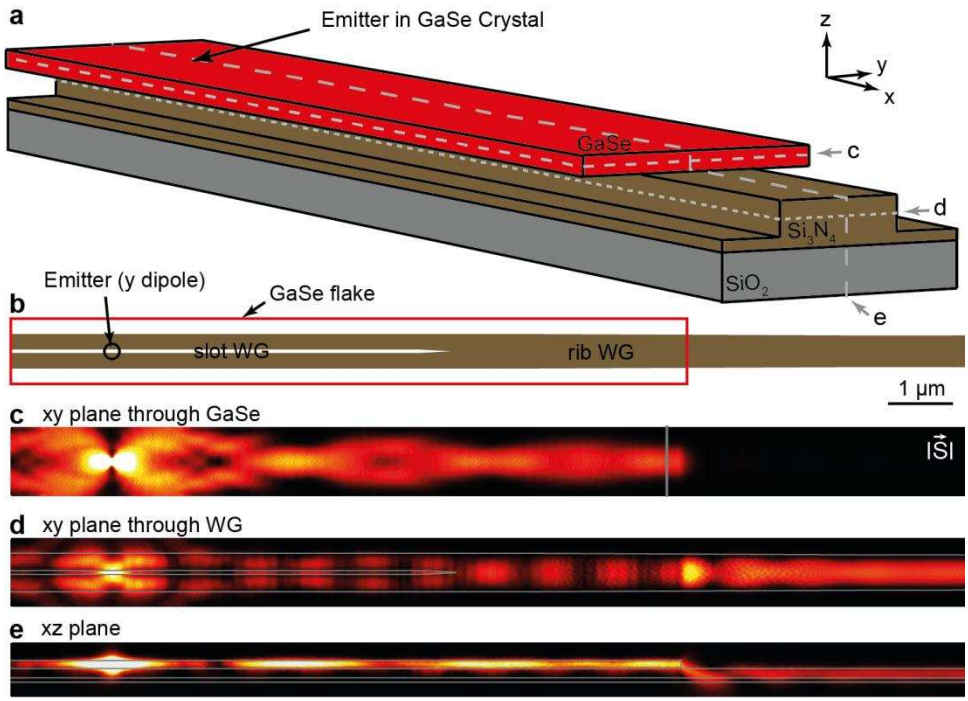

Figure S4. 3D simulation of the propagation of the emitted PL in the hybrid waveguide structure. (a,b) Sample structure of the 3D simulation of Fig. 3c in the manuscript. The GaSe crystal on top of the Si_3N_4 slot or rib waveguide has a size of 10 x 1 x 0.09 µm. The emitter (y dipole) is placed vertically centered inside the GaSe crystal and horizontally centered above the slot waveguide. (c-e) The calculated propagation of the emitted photoluminescence (PL) is depicted for different cross sections.

7. Calculated coupling efficiency of the emitters to the hybrid waveguide structure for different emitter positions and dipole orientations

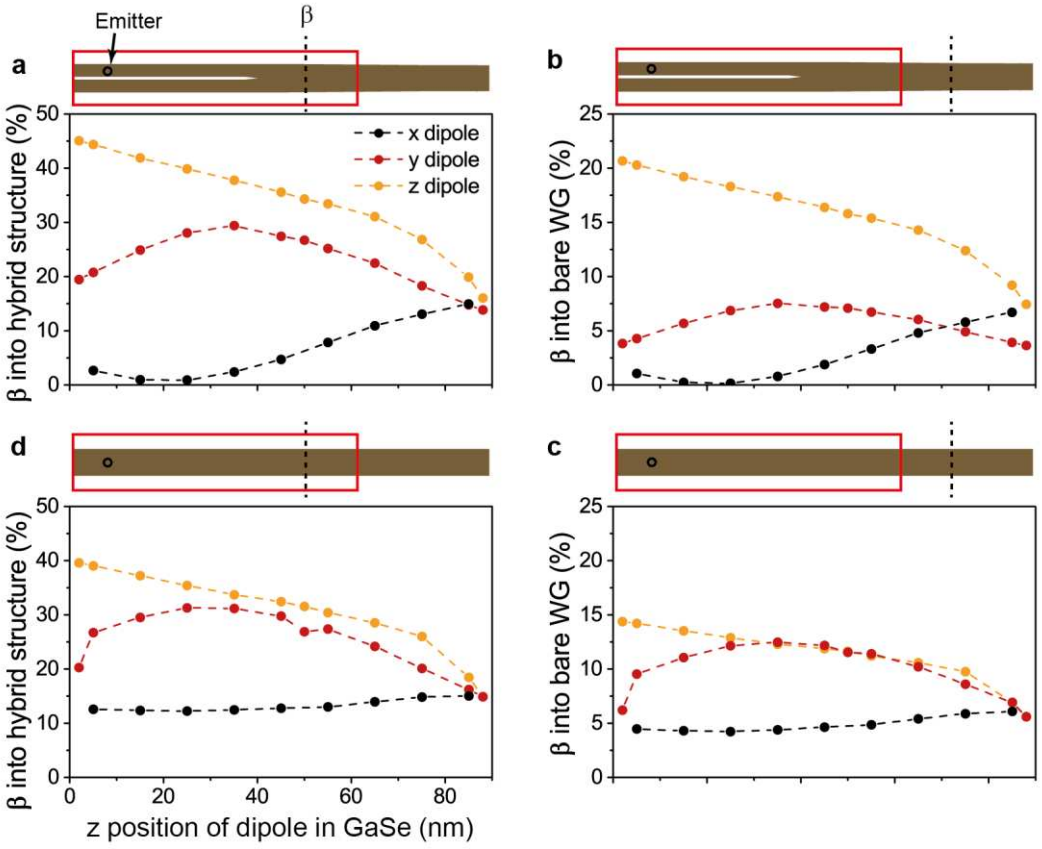

Figure S5. Calculation of the coupling efficiencies β of the emitters to the hybrid waveguide structure for different emitter positions and dipole orientations. The vertical black dotted lines in the schematic drawings indicate the positions, where the coupling efficiencies $\beta = I_{1D}/I_0$ into the GaSe/Si_3N_4 hybrid structure and the bare Si_3N_4 rib waveguide are calculated. I_0 is the total emitted light and I_{1D} the light confined in the hybrid structure or the bare waveguide. (a,b) Different coupling efficiencies to the waveguide are achieved, if the vertical position of the emitter is changed. For a slot waveguide the highest coupling efficiencies are reached for a z dipole near the GaSe/waveguide interface (z = 2 nm) and centered above one of the arms of the slot waveguide (see schematic drawing in the inset). (c,d). Coupling efficiencies for a rib waveguide and light emitters horizontally centered above the waveguide.

8. Experimental estimation of the coupling efficiency into the bare waveguide

A lower limit of the coupling efficiency can be estimated from the measured intensity of the emitter shown in Figure 3b in the main manuscript. As presented below in section 9, the intensity of the emitter in the waveguide is 35.2×10^6 cps. The photoluminescence life time of this emitter is 1 ns (obtained from the antibunching rise time in Figure 4). Thus, the total intensity cannot exceed

$(1\ \text{ns})^{-1} = 1\times10^9$ cps. This leads to a minimal coupling efficiency of $35.2\times10^6 / 1\times10^9 = 3.5$ % of this emitter. Since we do not operate the emitter in saturation, the true coupling efficiency should be higher.

9. Estimation of the internal quantum yield of the localized emitters in GaSe

We can make a rough estimate of the internal quantum yield (QY) using the detected light intensity of the emitters. The count rate of a single-photon emitter on one avalanche photodiode (APD) in the Hanbury-Brown and Twiss setup amounts to 4×10^3 cps. With the transmission efficiency of our setup of 4.5% and the detection efficiency of the APD of 40%, we can estimate that the objective lens collects an intensity of 220×10^3 cps at the emitter position. Considering that at the emitter position we only detect 1/160 of the intensity in the waveguide, a light intensity of 35.2×10^6 cps is present in the waveguide. The FEM simulations show that maximally 21% of the totally emitted light is collected by the waveguide, leading to a minimal intensity of the emitter of 167.6×10^6 cps. The approximate photoluminescence life time of the emitter can be extracted from the antibunching rise time and amounts to 1 ns. Thus, the maximum intensity of the emitter (in saturation) cannot exceed $(1\ \text{ns})^{-1} = 1\times10^9$ cps. This leads to a minimum internal quantum yield of the emitter of 17 %. However, the QY is most probably higher, since we did not measure the emitter in saturation. Furthermore, the precise position of the emitter with respect to the waveguide is unknown. As a consequence, the achieved coupling efficiency might be lower than 21%, and the QY would be higher then.

10. Photon correlation measurement under pulsed excitation

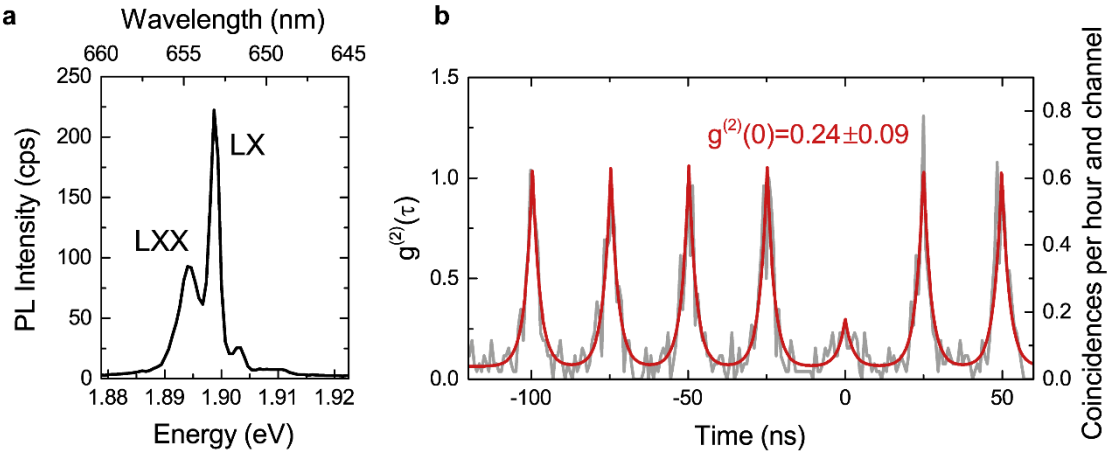

Figure S6. a) Spectrum of a quantum emitter in GaSe with exciton at 1.899 eV and biexciton at 1.894 eV. b) Photon correlation measurement $g^{(2)}(\tau)$ of the exciton line in (a) under pulsed excitation. The value $g^{(2)} = 0.24$ indicates single-photon emission. The red solid line represents the fit $g^{(2)}(\tau) = y_0 + \sum_n A_n e^{-|(\tau+nr)/\tau_0|}$ with $= 1/k_r$, where k_r is the repetition rate of the laser. A_n is the same for $-2 \leq n \leq 4$, except for $n = 0$. The emitter is excited with 200 fs pulses from a fiber laser system at a wavelength of 585 nm and with a repetition rate of 40 MHz. The integration time of the measurement is 5.5 hours with count rates of 800 cps on each APD of the HBT setup.